

Electron-lattice instabilities suppress cuprate-like electronic structures in SrFeO₃/SrTiO₃ superlattices

James M. Rondinelli* and Nicola A. Spaldin

Materials Department, University of California, Santa Barbara, CA, 93106-5050, USA

(Dated: November 7, 2018)

Using *ab initio* density functional theory we explore the behavior of thin layers of metallic d^4 SrFeO₃ confined between the d^0 dielectric SrTiO₃ in a superlattice geometry. We find the presence of insulating SrTiO₃ spacer layers strongly affects the electronic properties of SrFeO₃: For single SrFeO₃ layers constrained to their bulk cubic structure, the Fermi surface is two-dimensional, nested and resembles the hole-doped superconducting cuprates. A Jahn-Teller instability couples to an octahedral tilt mode, however, to remove this degeneracy resulting in insulating superlattices.

PACS numbers: 74.78.Fk;71.15.Mb;71.20.-b;71.30.+h;63.20.e

Progress in the layer-by-layer growth of transition metal oxide thin films [1, 2] motivated the intriguing recent suggestion that oxide heterostructures engineered to have band structures close to those of the high- T_c cuprates could yield new superconductors [3]. Strained LaNiO₃ layers separated by inert spacers such as LaAlO₃ or LaGaO₃ were proposed as a promising trial system, with strain lifting the degeneracy of the single Ni³⁺ e_g electron and layering providing quasi two-dimensionality. Indeed, first-principles electronic structure calculations [4] on strained Ni-based oxide superlattices have found that, with careful choice of strain and local-interface chemistry [5], 2D Fermi surfaces resembling those of the hole-doped cuprates [6] can be obtained. Superconductivity in such superlattices remains to be observed experimentally, however, possibly because competing instabilities such as charge- or orbital-ordering are enhanced by the reduced dimensionality. Although high- T_c superconductivity tends to occur in materials with large electronic fluctuations and in close proximity to electronic, structural or magnetic phase transitions [7, 8, 9, 10], the detailed role of such instabilities remains unclear [11, 12].

With these factors in mind, we examine how structural confinement and lattice instabilities modify the electronic structure of SrFeO₃ in SrTiO₃/SrFeO₃ superlattices. Our motivation for this choice of system is three-fold: First, like Ni³⁺, Fe⁴⁺ has a single degenerate e_g electron in an octahedral environment that dictates its low energy physics. The restriction on Fe-based compounds—traditionally dismissed from consideration for superconductivity because of their robust magnetism—has been lifted due to the recent discovery of superconducting Fe pnictides [13]. Second, bulk SrFeO₃ is metallic with p -type conductivity (like the doped cuprates) and is proximal to multiple instabilities: It manifests a long-wavelength spin density wave, but neither Jahn-Teller distorts nor charge orders, even though both possibilities are suggested by its chemistry. Finally, unlike the structurally inert LaAlO₃ in the nickelate superlattices, SrTiO₃ is a highly polarizable dielectric which can couple to electronic or structural distortions [14] in the SrFeO₃ layer.

Using first-principles density functional theory (DFT) within the local-spin density approximation (LSDA) plus Hubbard U method, we calculate the structure and electronic properties of (SrTiO₃) _{n} /(SrFeO₃) _{m} superlattices. We focus on (*i*) the evolution of the 2D band structure with thickness of the dielectric and metal ($n, m = 1$ or 3), and (*ii*) how competing structural and electronic instabilities manifest in the superlattices. We find that 2D confinement from the superlattice periodicity along the growth (z) direction yields low-energy physics that are primarily derived from hybridized Fe $d_{x^2-y^2}$ and O $2p$ orbitals. The idealized high-symmetry superlattice structure has a strongly nested 2D Fermi surface that is similar to that of the parent superconductor La₂CuO₄ [15]. Strong electron-lattice instabilities, enhanced by 2D confinement, transform the metastable metallic structure into a lower symmetry *insulating* superlattice. Understanding the competing nature of these often neglected lattice distortions is crucial for engineering electronic structures of oxide superlattices and interfaces.

Our LSDA+ U DFT calculations are performed using the Vienna *ab initio* Simulation Package (VASP) [16, 17]. We follow the Dudarev approach [18] and include an effective Hubbard term $U_{\text{eff}} = U - J$ of 6 eV to treat the Fe $3d$ orbitals [30]. This method and value of U_{eff} gave good results in earlier first-principles calculations for bulk SrFeO₃ and related iron oxide compounds [19, 20]. We construct the superlattices by stacking five-atom perovskite units along the z -direction [see Fig. 1(d)], and constrain the in-plane lattice parameter (xy -plane) to that of cubic LDA SrTiO₃ ($a = 3.86$ Å) to simulate growth on a SrTiO₃ substrate. While the lattice mismatch between SrFeO₃ and SrTiO₃ is small (the theoretical mismatch is 1.8%, with ferromagnetic LSDA+ U SrFeO₃ having $a = 3.79$ Å), we show below that it is sufficient to impose an epitaxial crystal field (Δ_{ECF}) that partially lifts the Fe e_g orbital degeneracy. We then relax the length of the c -axis and the internal degrees of freedom along the z -direction. The in-plane periodicity imposed by this choice of reference structure does not permit cell-doubling structural distortions such as octahedral rotations or orbital ordering: This

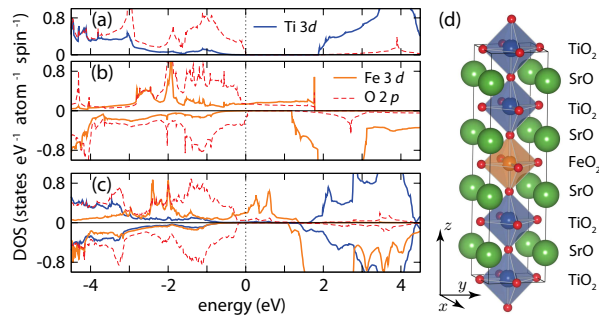


FIG. 1: (Color) The DOS for (a) cubic SrTiO₃ ($a = 3.86$ Å), (b) cubic FM SrFeO₃ ($a = 3.79$ Å), and (c) the high symmetry $P4/mmm$ (SrTiO₃)₃/(SrFeO₃)₁ superlattice shown in (d).

highly-symmetric superlattice (space group $P4/mmm$) resembles the structural constraints often considered to be imposed in heteroepitaxial thin films. We relax this restriction later to study electron-driven lattice instabilities. Ferromagnetic (FM) order is imposed on the Fe sites in all calculations, and is theoretically [20] found to be the lowest energy collinear ordering for bulk SrFeO₃.

We begin by studying the (SrTiO₃)₃/(SrFeO₃)₁ superlattice and plot in Figure 1 our calculated local densities-of-states (DOS) for (a) cubic SrTiO₃, (b) cubic SrFeO₃, and (c) the superlattice. Our results for the bulk compounds are consistent with the literature: In SrTiO₃ we obtain a ~ 2 eV band gap between an O 2p valence band and a Ti 3d conduction band. SrFeO₃ is nearly half-metallic with a calculated magnetic moment of $3.8 \mu_B$ per Fe atom, consistent with a high-spin d^4 electronic configuration. The Fermi level (dashed line at 0 eV) lies in a region of majority spin Fe e_g^\uparrow -O $2p^\uparrow$ hybridized orbitals and in the O $2p^\downarrow$ valence band. The electronic structure of the superlattice is close to a superposition of its constituents, except for a reduction in the contribution of the O 2p states at E_F making the superlattice half-metallic. While the use of the Hubbard U method in DFT calculations is known to drive bands toward integer filling, the half-metallicity is robust for $U = 0$ to 8 eV.

We plot the band structure of the $P4/mmm$ superlattice in Figure 2(a,b) using the “fat-band” method [21] in which the magnitude of the projection of each Bloch state onto a particular set of atomic orbitals is represented by its line width: Panel (a) shows the equatorial O $2p_{x,y}$ -Fe $3d_{x^2-y^2}$ states and (b) shows the O $2p_z$ -Fe $3d_{z^2}$ orbitals. Consistent with the DOS, we find partial occupation of the majority $d_{x^2-y^2}$ and d_{z^2} Fe states at E_F with the energy of the $d_{x^2-y^2}$ at Γ 0.50 eV lower than that of the d_{z^2} orbital. The energy difference at Γ is explained from compression of the apical (1.88 Å) over the in-plane (1.93 Å) Fe-O bond length from the imposed Δ_{ECF} [4]. Interestingly, the apical Fe-O distance is shorter than the value (1.90 Å) that we obtain when we force *bulk* SrFeO₃ to have the SrTiO₃ in-plane lattice constant, suggestive of

an additional spontaneous Jahn-Teller-like distortion (we examine this later). Despite the substrate elongation of the equatorial Fe-O bonds, the bands of $d_{x^2-y^2}$ character do not fully split from the d_{z^2} bands to produce a single band crossing E_F ; in fact, both the top and the bottom of the e_g band are dominated by $d_{x^2-y^2}$ states. The d_{z^2} band can likely be further destabilized to achieve an identical cuprate-like electronic structure with additional strain [3] and/or chemical modifications [4].

We now investigate the character of the 2D bands and examine how the electronic structure at E_F responds to changes in the dielectric thickness by comparing the full band structures of the (SrTiO₃)₃/(SrFeO₃)₁ [Fig. 2 (a,b)] and (SrTiO₃)₁/(SrFeO₃)₁ [(c,d)] superlattices. As expected, the bandwidth of the $d_{x^2-y^2}$ derived states along Γ -A is nearly the same in the two superlattices due to identical in-plane structural parameters. The dispersion of the d_{z^2} bands is markedly different, however, with the less confined $n = 1, m = 1$ superlattice having a larger bandwidth than the more confined $n = 3, m = 1$ along the M-A lines. Increasing dielectric thickness ($n = 1 \dots 4$) shows that the dispersive $d_{x^2-y^2}$ bands saturate at ~ 2 eV in width while the d_{z^2} states are almost dispersionless, although never fully split. In contrast, increasing the thickness of the SrFeO₃ layers in the superlattice produces several partially occupied e_g bands crossing E_F , and the band structure (not shown) resembles a regular metal. We conclude that a cuprate-like band structure is unlikely in superlattices containing multiple ferrate layers.

The 2D confinement is discernible in the Fermi surface of the $n = 3, m = 1$ superlattice shown in Fig. 2(e,f). The additional band crossing E_F in the $k_z = 0$ plane,

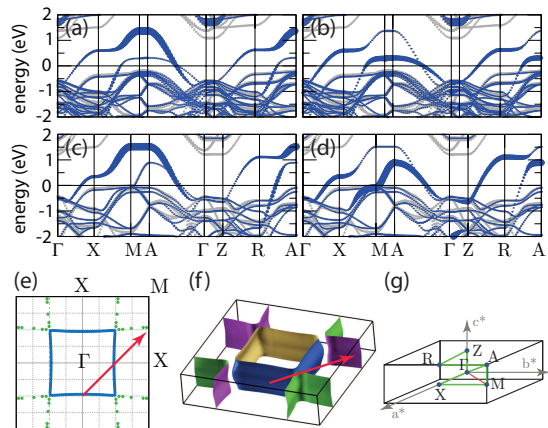


FIG. 2: (Color) Electronic band structure plots for the $n = 3, m = 1$ [panels (a) and (b)], and $n = 1, m = 1$ [panels (c) and (d)] superlattices. Panels (a) and (c) show the majority spin “fat-bands” (blue) derived from O $2p_{x,y}$ -Fe $3d_{x^2-y^2}$ states, whereas (b) and (d) show the O $2p_z$ -Fe $3d_{z^2}$ states. The Fermi surface at $k_z = 0$ (e) and in the full (f) BZ shown in (g) consists of two bands connected by the $\mathbf{Q} = (1, 1, 0)\frac{\pi}{a}$ interband nesting vector (arrow).

not seen in the $n = 1, m = 1$ (c,d) superlattice nor bulk SrFeO₃ lattice matched to SrTiO₃, produces squared-cylindrical arrays around the M-point consistent with the four-fold symmetry of the lattice. An unusual inward bowing along the Γ -X direction occurs with corrugations along k_z similar to over-doped cuprates. The band curvature indicates electron and hole sheets at Γ and M, respectively, similar in character to the superconducting cuprates [15, 22]. Interestingly, the two Fermi sheets nearly intersect at half the Γ -M distance producing a nesting vector $\mathbf{Q} = (1, 1, 0)\frac{\pi}{a}$ connecting them. Such a vector can result in a charge or spin density wave, or for strong coupling of the electronic system to the lattice, a symmetry lowering structural distortion. These two sheets are largely insensitive to the calculation details: changing U weakly affects the band crossings at E_F since the electronic structure is mainly modified by the confining SrTiO₃ layers. Spin-orbit interactions also do not alter the FS nesting.

We now investigate possible structural instabilities in the (SrTiO₃)₃/(SrFeO₃)₁ superlattice, and their influence on the FS degeneracy. We identify likely M-point instabilities (consistent with the nesting vector) by choosing structural distortions that connect the high symmetry reference phase to low symmetry structures through atomic distortions that maintain a direct group-subgroup relation. We choose these distortions [23] to be irreducible representations (irreps) of space group $P4/mmm$ and consider only M_i^+ , for $i = 1 \dots 5$. (We ignore M_i^- irreps with antisymmetric distortions under inversion, and follow the notation of Miller & Love throughout [24].) Fully relaxed *ab initio* structures are then reduced into combinations of these irreps by performing a symmetry mode analysis [25] that makes accessible the local atomic displacements. We keep FM spin order fixed as above to isolate the electron-lattice coupling.

The active irreps we examine (Fig. 3) affect either the equatorial Fe-O bond lengths (crystal field) or O-Fe-O bond angles ($dp\sigma$ bandwidth). Irreps M_1^+ and M_2^+ are planar breathing and stretch modes of the FeO₄ plaquettes, respectively, and are anticipated to strongly modulate the e_g^1 -O $2p$ hybridization at E_F . The M_1^+ mode produces two unique FeO₄ plaquettes arranged in a 2D checkerboard manner and gives rise to charge disproportionation in bulk isoelectronic CaFeO₃ [26]. In contrast the M_2^+ irrep, or Jahn-Teller mode, creates two long and two short equatorial Fe-O bonds and favors orbital polarization. The remaining irreps are collective distortions of the octahedral units that produce the common tilt and rotation patterns found in perovskite oxides. These modes affect the $dp\sigma$ bandwidth through deviations in the Fe-O-Fe bond angle away from ideal 180°: M_3^+ consists of rotations of the in-plane oxygen atoms about the z -axis; M_4^+ produces a bending distortion of the O-Fe-O bond; and the 2D irrep M_5^+ produces two possible tilt patterns of the planar oxygen atoms: $M_5^+(a,0)$ giving a pattern with

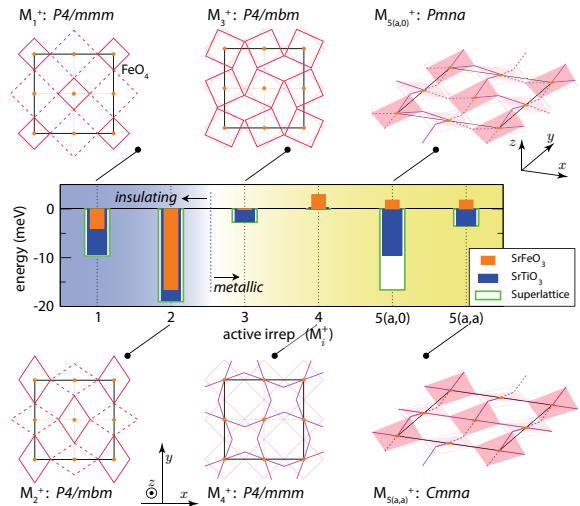


FIG. 3: (Color) Electronic responses from SrFeO₃ (orange), SrTiO₃ (blue), and the superlattice (green) to M_i^+ irreps of space group $P4/mmm$: M_1^+ breathing mode, M_2^+ stretch mode, M_3^+ rotation mode of the FeO₆ octahedra around the z -direction, M_4^+ bending of the Fe-O bonds (purple), and two different tilt patterns $M_5^+(a,0)$ and $M_5^+(a,a)$ in the xy -plane.

space group symmetry $Pmna$ or $M_5^+(a,a)$ with $Cmma$.

We begin by “freezing” each irrep as a function of mode amplitude into the equatorial oxygen atoms coordinating Fe (see Supp. Materials). At the same time, we keep the remaining atoms in the superlattice clamped to the reference $P4/mmm$ positions to isolate the response of the ferrate layer—displacements of other atoms in the superlattice are obtained later through full structural optimization. The energy change due to the optimal mode amplitude for each irrep frozen in the ferrate layer is shown in Fig. 3 with respect to the high symmetry $P4/mmm$ superlattice (energies per five-atom perovskite cell). Irreps M_1^+ , M_2^+ and M_3^+ lower the energy of the *superlattice*. In contrast they increase the energy of *bulk* SrFeO₃ lattice matched to SrTiO₃, indicating that the superlattice geometry makes the e_g orbital degeneracy more susceptible to structural distortions. The remaining irreps which require collective cooperation of all oxygen octahedra increase the superlattice energy when the dielectric is clamped to the reference configuration. Next, we fully relax the SrTiO₃ with the ferrate atoms fixed to the distortions above to isolate the effect of the dielectric response. Now every irrep except M_4^+ is found to be energy lowering: the large energy gain now observed for the M_5^+ modes suggests that a 3D tilt pattern is preferred—this result is likely driven by the fact that most of the superlattice is SrTiO₃ which itself has a large M_5^+ -like mode instability.

We now relax both constituents under the symmetry constraints imposed by the irreps to find the lowest energy atomic configurations. The largest energy-lowering distortions are found to be the Jahn-Teller and tilt modes.

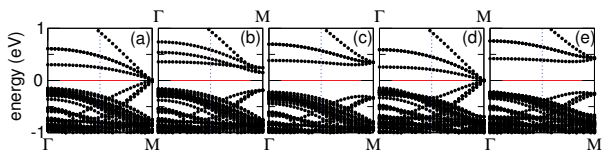


FIG. 4: Band structure for (a) the $P4/mmm$ ($n = 3, m = 1$) superlattice as in Fig. 2(a) with the lattice parameter doubled in-plane to allow comparison with panels (b)-(d) which include additional structural distortions: (b) M_1^+ , (c) M_2^+ , and (d) $M_5^+(a, 0)$; and the ground state $P2_1/c$ structure (e).

Both irreps M_1^+ and M_2^+ open energy gaps at the Fermi level in the superlattice [Fig. 4(b,c)], while identical distortions in bulk SrFeO_3 maintain its metallicity. The tilt modes $M_5^+(a, 0)$ and $M_5^+(a, a)$ are more unstable than the rotation M_3^+ irrep with $M_5^+(a, 0)$ almost as energetically favorable as the Jahn-Teller distortion. Yet, due to the weaker influence of the bond angle on the $d\rho\sigma$ bandwidth, none of the bond angle distortions gap the FS. There is a 0.24 eV bandwidth reduction, however, for irrep M_5^+ shown in Fig. 4(d). Similarly, the M_1^+ mode also gaps the Fermi surface—although not an energy lowering distortion—in doped La_2CuO_4 , whereas the octahedral tilt and rotation modes, which are found in the cuprates, show minor effects [27].

Finally, we calculate the fully optimized structure starting from a combination of the M_2^+ and M_5^+ irreps. Our ground state structure is 33.5 meV lower in energy (per 5-atom unit cell) than the reference superlattice. It contains FeO_4 plaquettes with bond lengths of 1.86 and 2.01 Å due to the Jahn-Teller mode that makes the superlattice insulating [0.58 eV gap, Fig. 4(e)]. The octahedral instabilities largely condense in the SrTiO_3 layers with reduced interaction in the ferrate plane: The in-plane Fe–O–Fe bond angle is reduced by 6.89° while a 10° reduction occurs across the Fe–O–Ti angle. By symmetry decomposing the structure as a combination of the $P4/mmm$ irreps, $0.051\Gamma_1^+ + 0.048\Gamma_5^+ + 0.21M_2^+ + 0.13M_3^+ + 0.97M_5^+$, we find the primary order parameters M_2^+ and M_5^+ drive the $P4/mmm$ (a^0, a^0, c^0) \rightarrow $P2_1/c$ (a^+, b^-, b^-) metal-insulator transition, with the associated change in octahedral tilt patterns. Since none of these distortions are favored in bulk SrFeO_3 , we attribute the electron-lattice coupling enhancement to the confinement effects imposed by the superlattice geometry.

We have demonstrated that in a superlattice geometry, confinement from dielectric spacer layers combines with a strain-induced epitaxial crystal field (Δ_{ECF}) to modify the energies and dispersions of apical d_{z^2} and in-plane Fe $d_{x^2-y^2}$ orbitals. When we simulate the high symmetry cubic structures of room temperature SrTiO_3 and SrFeO_3 partial planar electron localization yields a 2D Fermi surface that resembles the superconducting cuprates. Low-energy M-point instabilities compete with nesting on the Fermi surface to make the superlattices

proximal to multiple competing phases. The lattice instabilities are enhanced by the dielectric SrTiO_3 layers, therefore inert spacer layers without polarizable ions might be more favorable for superconductivity. We hope that our finding of competing structural ground states with distinct electronic properties motivates experimental investigation of $\text{SrFeO}_3/\text{SrTiO}_3$ heterostructures using external electric and magnetic fields: Such probes could tune between the itinerant and localized electronic states in analogy with the parent Mott insulating cuprates.

We gratefully acknowledge support from NDSEG (JMR), the NSF under grant no. DMR 0940420 (NAS), and discussions with C. Adamo and K. Delaney.

* Address correspondence to: rondo@mrl.ucsb.edu

- [1] H. Y. Hwang, *Science* **313**, 1895 (2006).
- [2] J. W. Reiner, et al., *Science* **323**, 1018 (2009).
- [3] J. Chaloupka, et al., *Phys. Rev. Lett.* **100**, 016404 (2008).
- [4] P. Hansmann, et al., *Phys. Rev. Lett.* **103**, 016401 (2009).
- [5] O. Andersen, APS March Meeting (2009), URL <http://meetings.aps.org/link/BAPS.2009.MAR.Q30.4>.
- [6] E. Pavarini, et al., *Phys. Rev. Lett.* **87**, 047003 (2001).
- [7] E. Morosan, et al., *Nat. Phys.* **2**, 544 (2006).
- [8] A. D. Bianchi, et al., *Science* **319**, 177 (2008).
- [9] N. Nagaosa, *Science* **275**, 1078 (1997).
- [10] C. de la Cruz, et al., *Nature* **453**, 899 (2008).
- [11] V. J. Emery, et al., *Nature* **374**, 434 (1995).
- [12] P. B. Allen, in *Dynamical Properties of Solids*, edited by G. K. Horton, et al. (North-Holland, New York, 1980), vol. 3, pp. 95–196.
- [13] Y. Kamihara, et al., *J. Amer. Chem. Soc.* **130**, 3296 (2008).
- [14] S. Okamoto, et al., *Phys. Rev. Lett.* **97**, 056802 (2006).
- [15] R. E. Cohen, et al., *Phys. Rev. Lett.* **60**, 817 (1988).
- [16] G. Kresse, et al., *Phys. Rev. B* **54**, 11169 (1996).
- [17] G. Kresse, et al., *Phys. Rev. B* **59**, 1758 (1999).
- [18] S. L. Dudarev, et al., *Phys. Rev. B* **57**, 1505 (1998).
- [19] T. Saha-Dasgupta, et al., *Phys. Rev. B* **72**, 045143 (2005).
- [20] I. Shein, et al., *Phys. Sol. State* **47**, 2082 (2005).
- [21] O. Jepsen, et al., *Z. Phys. B* **97** (1995).
- [22] W. E. Pickett, et al., *Phys. Rev. B* **42**, 8764 (1990).
- [23] B. J. Campbell, et al., *J. Appl. Cryst.* **39**, 607 (2006).
- [24] S. Miller, et al., *Tables of Irreducible Representations of Space Groups and Co-Representations of Magnetic Space Groups* (Pruett, Boulder, 1967).
- [25] M. I. Aroyo, et al., *Acta Cryst* **A62**, 115 (2006).
- [26] J. Matsuno, et al., *Phys. Rev. B* **66**, 193103 (2002).
- [27] L. F. Mattheiss, *Phys. Rev. Lett.* **58**, 1028 (1987).
- [28] P. E. Blöchl, *Phys. Rev. B* **50**, 17953 (1994).
- [29] H. J. Monkhorst, et al., *Phys. Rev. B* **13**, 5188 (1976).
- [30] The core and valence electrons are treated with the projector augmented wave method [28] with the following valence electron configurations: $3s^23p^64s^2$ (Sr), $3p^63d^74s^1$ (Fe), $3s^23p^63d^24s^2$ (Ti) and $2s^22p^4$ (O). The Brillouin zone integrations are performed with a Gaussian smearing of 0.05 eV over a $9 \times 9 \times 5$ Monkhorst-Pack k -point mesh [29] centered at Γ , and a 450 eV plane-wave cutoff. For structural relaxations, we relax the ions until the Hellmann-Feynman forces are less than $1 \text{ meV } \text{Å}^{-1}$.